

Attenuated cooling effects with increasing water-saving irrigation: Satellite evidence from Xinjiang, China



Chao Zhang^{a,b}, Jinwei Dong^{a,*}, Guoyong Leng^c, Russell Doughty^d, Kun Zhang^{e,f}, Songjun Han^{g,h}, Geli Zhangⁱ, Xuezhen Zhang^a, Quansheng Ge^{a,*}

^a Key Laboratory of Land Surface Pattern and Simulation, Institute of Geographic Sciences and Natural Resources Research, Chinese Academy of Sciences, Beijing 100101, China

^b University of Chinese Academy of Sciences, Beijing 100049, China

^c Key Laboratory of Water Cycle and Related Land Surface Processes, Institute of Geographic Sciences and Natural Resources Research, Chinese Academy of Sciences, Beijing 100101, China

^d GeoCarb Mission, College of Atmospheric and Geographic Sciences, University of Oklahoma, OK 73019, United States

^e Department of Mathematics, The University of Hong Kong, Hong Kong 999077, China

^f School of Biological Sciences, The University of Hong Kong, Hong Kong 999077, China

^g State Key Laboratory of Simulation and Regulation of Water Cycle in River Basin, Institute of Water Resources and Hydropower Research, Beijing 100038, China

^h National Center of Efficient Irrigation Engineering and Technology Research, Beijing 100038, China

ⁱ College of Land Science and Technology, China Agricultural University, Beijing 100193, China

ARTICLE INFO

Keywords:

Water-saving irrigation
Xinjiang
Land surface temperature
Water use
Weakened cooling effect

ABSTRACT

The cooling effects of agricultural irrigation on land surface temperature (LST) are more evident in arid areas like Xinjiang Uygur Autonomous Region (Xinjiang) in northwest China. In the 21st century, irrigation practices improved, and the water-saving irrigation (WSI) area increased substantially from 1266 ha in 2000 to 2916 ha in 2019. However, it remains unclear how the cooling effects changed along with the increasing WSI area relative to traditional irrigation. Here we examine the changes in irrigation cooling effects on LST in Xinjiang from 2000 to 2020 at multi-spatiotemporal scales and analyze their relationship with irrigation water use (IWU). We find a significant decrease in daytime cooling effects (0.21 K/decade) but an increase in nighttime cooling (0.17 K/decade) over stable croplands in Xinjiang, both of which significantly ($P < 0.05$) correlate to the decreased IWU. Seasonally, the weakened daytime cooling effect is most evident in late summer and early spring. Spatially, the decrease in the cooling effects is much more prominent in South Xinjiang (0.48 K/decade, $p < 0.05$) than in North Xinjiang, possibly due to their different WSI extents, intensities, and climate conditions (e.g., precipitation). Furthermore, we identify different cooling alleviation trends in two different agricultural systems: state farms with more advanced WSI measurements and conventional farms with fewer WSI infrastructures. We find that the state farms had a higher LST (Δ LST: 0.60 K) and vapor pressure deficit (Δ VPD: 0.013 kPa) than conventional farms in 2000, but that gap significantly decreased to 0.32 K and 0.002 kPa in 2020 due to increasing WSI in conventional farms, suggesting that the promotion of WSI dampened the irrigation cooling effects in Xinjiang. Our findings show that WSI lessens the cooling effect of irrigation, and we suggest that WSI-related effects on temperature should be considered in climate modeling and climate change scenarios.

1. Introduction

Irrigated agriculture constitutes about 40% of global food production, comprises 18% of global croplands, and consumes more than 60% of freshwater withdrawals (Bin Abdullah, 2006; Puma and Cook, 2010; Wu et al., 2022a; Zhang et al., 2022f). As one of the most pervasive

human activities, irrigation has a pronounced impact on earth surface properties, land-atmosphere interactions, hydrological cycles, and climate changes (Kueppers et al., 2007; Lobell and Bonfils, 2008; Sacks et al., 2009; Shen et al., 2021), by conveying water from rivers, lakes and underground to croplands (Puy et al., 2021). Some biophysical factors like ground surface albedo, soil and vegetation evapotranspiration (ET),

* Corresponding authors.

E-mail addresses: dongjw@igsnrr.ac.cn (J. Dong), geqs@igsnrr.ac.cn (Q. Ge).

and aerodynamics have been changed by large-scale irrigation practices, and thus the irrigation effect on regional climate attracted increasing attention (Ambika and Mishra, 2019; Liu et al., 2021; Nocco et al., 2019; Wang et al., 2021b; Zhang et al., 2017c). The irrigation effect on climate is more evident in arid regions like Xinjiang Uygur Autonomous Region (hereafter Xinjiang) in northwest China where crop growth heavily depends on irrigation (Zhang et al., 2022e, 2022d). The accelerated expansion of croplands with a heavy dependence on irrigation has not only stressed local water resources but has also significantly altered regional climate by reducing land surface temperature (LST) and enhancing precipitation (Zhang et al., 2020b; Zhou et al., 2016, 2021a).

Numerous studies have reported that irrigation cooled near-surface or land surface temperature by enhancing evapotranspiration and reducing albedo using in situ measurements (Lobell and Bonfils, 2008; Mahmood et al., 2004; Nocco et al., 2019), satellite observations (Yang et al., 2020b; Zhang et al., 2022g; Zhang et al., 2023), and model simulations and control experiments (Ambika and Mishra, 2021; Lobell et al., 2009; Lu et al., 2017; Thiery et al., 2020; Zhang et al., 2017c). For instance, Mahmood et al. (2006) found that irrigation resulted in 1 K cooling during the post-1945 years based on comparisons of near-surface air temperatures between irrigated and non-irrigated sites in the northern Great Plains, USA. Yang et al. (2020a) reported that irrigation cooled daytime LST by 1.15 K and nighttime LST by 0.13 K across China using pairwise comparison of satellite observations of irrigated and nearby non-irrigated areas in the same year. Using a coupled land-atmospheric simulation with the Weather Research and Forecast (WRF) model, Zhang et al. (2017c) found the daily mean temperature decreased by 1.7 K and humidity increased by 2.3 g kg^{-1} because of irrigation in the Heihe River Basin, northwest China. So far, the cooling effect of irrigation and its biophysical mechanisms have been thoroughly studied (Liu et al., 2021, 2022; Wang et al., 2021b; Zhang et al., 2017c, 2022g). However, most previous studies were based on a static irrigation map and did not consider the effects of changes in irrigation methods on climate, such as water-saving irrigation (WSI) practices and technologies, which impedes our understanding of how irrigation-climate feedbacks are changing.

WSI techniques like drip and sprinkler irrigation are effective to promote agricultural sustainability by increasing water use efficiency while maintaining or even increasing crop yields (Molden et al., 2010; Xu et al., 2018; Yang et al., 2023; Zhang et al., 2017a; Zhou et al., 2021b). It is estimated that the non-beneficial water consumption across the world's river basins can be reduced by 54% and 76%, respectively, by replacing surface irrigation with sprinkler and drip systems (Jägermeyr et al., 2015). As one of the most water-scarce countries, China experienced rapid development of WSI and thus reduced irrigation water use per hectare by ~30% during the last two decades (Ministry of Water Resources, 2021). In arid northwest China where mean annual precipitation is less than 200 mm (Yao et al., 2022a), the promotion of WSI has greatly contributed to the continuous agricultural expansion by reducing the crop water stress (Fu et al., 2022b). WSI techniques were first tested in the late 1970s by the Xinjiang Production and Construction Corps (XPCC) (Zhao et al., 1996) and were gradually promoted to the whole of Xinjiang after 1998 (Deng et al., 2006; Zhang et al., 2014; Zhong et al., 2009, 2016). As a result, the WSI area expanded by 130%, and the mean water use per hectare decreased by over 26% since the 21st century (Yang, 2019). Further, several studies reported that the promotion of WSI in northwest China has led to the reduction of ET, soil moisture, and relative air humidity, and thus producing non-negligible impacts on local and regional climate (Fu et al., 2022b; Han et al., 2021, 2017a; Kamran et al., 2023; Wang et al., 2022).

Thus, the expansion of WSI raises an important question: Was the cooling effect of irrigation reduced or even reversed with the promotion of WSI? Yao et al. (2022b) argued that different irrigation methods (e.g., flood, sprinkler, and paddy techniques) have different effects on surface fluxes despite the small magnitudes, simulated by incorporating six different irrigation schemes in Community Land Model. A study based

on WRF model simulations indicated that switching from conventional (channel) to efficient (drip) irrigation leads to moderate warming (~0.2 K) over the Indo-Gangetic Plain (Ambika and Mishra, 2022). Using long-term observations from meteorological stations at controlled and irrigated sites, Fu et al. (2022a) found that the large-scale application of WSI techniques in northwest China increased growing-season air temperature by 0.3 K and reduced relative humidity by 2%. However, existing studies were susceptible to the uncertainties of model parameterization or cannot be upscaled to broad regions to represent spatial discrepancies. On the one hand, different regions like North and South Xinjiang had different development stages and varied WSI intensities (Qi et al., 2022; Zhou et al., 2020); on the other hand, different climate backgrounds (e.g., precipitation and air temperature) may differ a lot in affecting the irrigation cooling effects (Chen and Dirmeyer, 2019; Yang et al., 2020a). Satellite observations may provide us an alternative to study to what extent the increasing WSI has affected the irrigation cooling effect across Xinjiang, considering both spatial and temporal discrepancies.

Here we first made two hypotheses: 1) the irrigation cooling effects have changed in Xinjiang in the last two decades and this change has spatial and temporal patterns; and 2) the expansion of WSI negatively affected irrigation cooling trends due to less water use. Second, we conducted two analyses to test our hypotheses: 1) we extracted the cooling effects of stable irrigated croplands and examined their trends at the pixel scale, and investigated the relationship between the cooling trend and changes in water use at the regional scale (i.e., North and South Xinjiang); and 2) we compared the climatic difference between farmlands inside and outside of XPCC farms, which have different WSI development stages (early development inside of XPCC since the 1970s and late promotion outside of XPCC after 1998), and observed whether the differences were minimized due to the increased WSI area outside of XPCC. Our findings could advance our understanding of how changes in irrigation practices impact the climate in Xinjiang.

2. Materials and methods

2.1. Study area

Xinjiang is in northwest China, has a total area of $1.66 \times 10^6 \text{ km}^2$, and spans from the Pamir and the Western Tianshan Mountains in the west to the Gobi Desert in the east, and from the Altai Mountains in the north to the Kunlun Mountain in the south. Xinjiang is covered by extensive deserts, oases, mountain glaciers, and snow cover. The terrain of Xinjiang is characterized by three mountain ranges that surround the two desert basins (Fig. 1), which creates a unique mountain-basin system with distinct hydrological processes. Xinjiang has a typical inner-continental dry climate and is one of the aridest regions in the world. Annual precipitation is less than 200 mm (Fig. S2) but potential ET ranges from 1600 to 2300 mm (Han and Yang, 2013). Xinjiang is an important crop and grain base and produces a lot of wheat, maize, cotton, vegetables, and other grain and cash crops (Zhang et al., 2022a). Almost all crops in Xinjiang rely heavily on irrigation, which usually lasts from May to September (Zhang et al., 2022b, 2022c). In addition, irrigation is also implemented during early spring and winter for salt leaching and the conservation of soil moisture (Han and Yang, 2013). Under the background of global warming, the oasis economy and desert ecology in Xinjiang are particularly fragile and acute due to the overuse of water resources (Yao et al., 2022a). In recent decades, WSI techniques were widely promoted in Xinjiang to enhance water use efficiency and reduce the heavy dependence of agriculture on snow and glacier melt, exerting non-negligible climatic effects (Fu et al., 2022b).

2.2. Data

2.2.1. Land use and land cover data

We acquired the NLCD (National Land Cover Dataset of China)

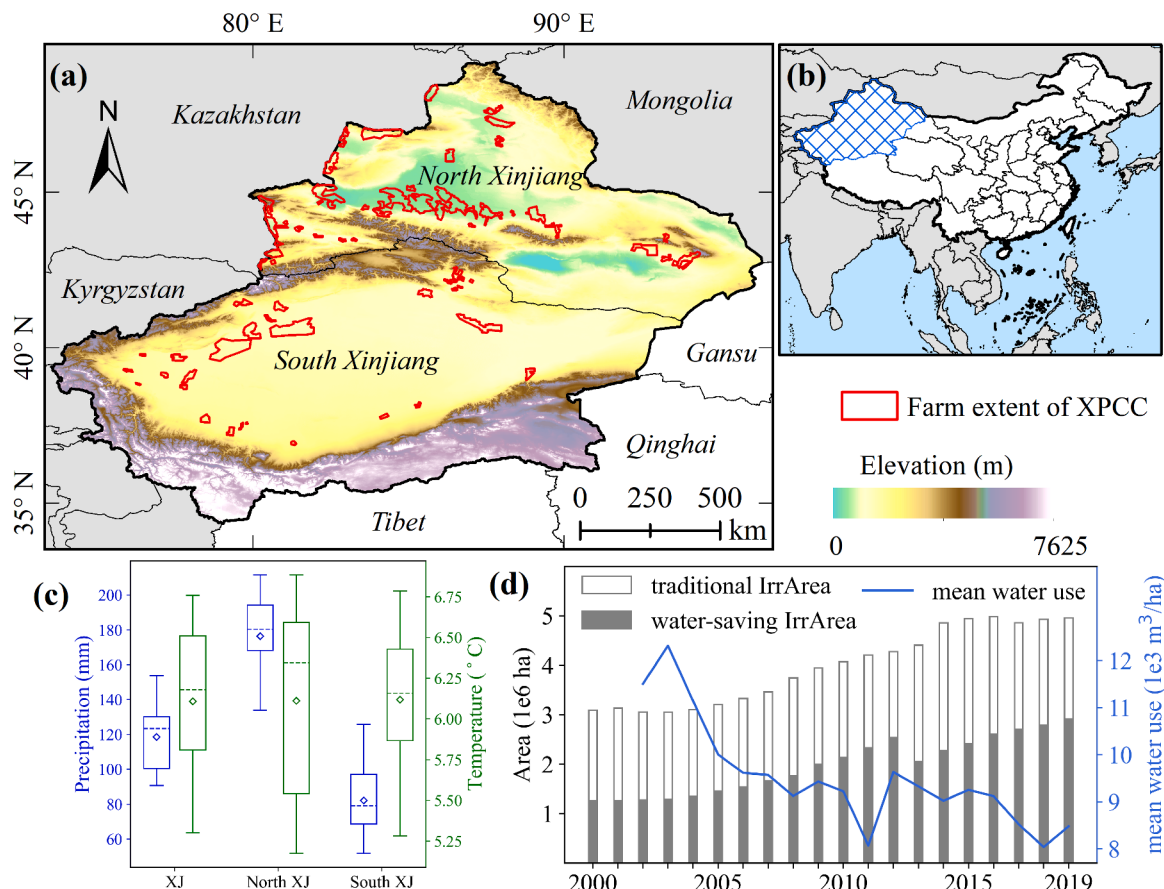


Fig. 1. The digital elevation model (DEM) of Xinjiang (XJ) (a) and the location of XJ in China (b). (c) Precipitation and temperature of XJ, South XJ, and North XJ derived from TerraClimate (Abatzoglou et al., 2018) from 2000 to 2020. (d) The traditional irrigation area (hollow bar), water-saving irrigation area (solid bar), and mean water use for irrigation (blue line) for XJ. IrrAera = Irrigation area, XPCC = Xinjiang Production and Construction Corps.

dataset from the Data Center for Resources and Environmental Sciences of the Chinese Academy of Sciences (<https://www.resdc.cn>). This dataset was generated every five years since the 1980s using visual interpretation of Landsat imagery and has an accuracy of over 90% (Liu et al., 2014, 2005, 2010), and has been widely used in various studies (Xin et al., 2020; Zhang et al., 2017b, 2020a). There are six first-level land cover types (i.e., cropland, forest, grassland, water, construction land, and unused land) in the NLCD with three spatial resolutions (i.e., 30 m, 100 m, 1000 m). Here we adopted the 1-km dataset from the 1980s to 2020.

2.2.2. MODIS LST and TerraClimate data

We used the 8-day LST data with 1 km resolution from MOD11A2 (Terra), calculated through a split-window algorithm using MODIS emissivity bands 31 and 32 (Wan, 2008), as the primary data. The LST data include daytime (local solar time ~ 10:30 a.m.) and nighttime (~10:30 p.m.) observations under the clear sky from 2000 to 2020. To ensure only high-quality and cloud-free pixels were used, we filtered the LST products using the quality control (QC) layers. Only “good quality data” and “other quality data” but with “average emissivity error ≤ 0.02 ” and “average LST error ≤ 1 K” were selected (Li et al., 2015). TerraClimate with a spatial resolution of 4000 m is a dataset of monthly climate and climatic water balance for global terrestrial surfaces and combines the WorldClim dataset, CRU Ts4.0, and JRA55 using climatically aided interpolation (Abatzoglou et al., 2018). The dataset has been widely used in multi-discipline studies including climate changes (Li et al., 2022; Wu et al., 2022b), hydrological cycles (Stahl and McColl, 2022), and ecological evaluations (Kitzberger et al., 2022). Based on our validation (see Text S1 and Fig. S1 for more details), the TerraClimate

had a satisfactory performance in Xinjiang and could be used to do the attribution analyses of Δ LST changes and to investigate the different climate effects of traditional and water-saving irrigation. All of these data sets were extracted from the Google Earth Engine platform (Gorelick et al., 2017) and averaged to monthly and annual values, except annual precipitation which was accumulated from monthly data.

2.2.3. Other data sets

We used the Shuttle Radar Topography Mission (SRTM) digital elevation model (DEM) dataset with 90 m resolution (Jarvis, 2008) to extract the valid grids (excluding the topographic effects) when investigating the irrigation cooling effects. The distribution map of XPCC farms was obtained from the Bureau of Natural Resources of XPCC and was digitized into shapefile format in ArcGIS. Agricultural water use data was from the Water Resources Bulletin of Xinjiang from 2002 to 2019. We also used air temperature from the Peng_1 km dataset (Peng et al., 2019) to examine the temperature difference between farms inside and outside of XPCC, corroborating the findings derived from the TerraClimate. The air temperature (Peng_1 km) with a resolution of 0.5 arcmins (~1 km) was spatially downscaled from CRU TS v402 using Delta downscaling method from 1901 to 2020 and was validated as reliable in China (Peng et al., 2019). All raster data in this study were resampled to 1000 m, using the nearest neighbor sampling method (Table 1).

2.3. Methods

The workflow of this study is illustrated in Fig. 2.

Table 1

The data sets used in this study. NLCD = National Land Cover Dataset of China, LST = Land surface temperature, Ta = Air temperature. ET_a and ET_r represent actual and reference evapotranspiration, respectively. VPD = Vapor Pressure Deficit. SM = Soil moisture, SR = Solar radiation.

Dataset	Resolution	Temporal period	Type	Reference
NLCD	1000 m	1980s-2020 (5-year interval)	Land use and land cover	Liu et al. (2014)
MOD11A2	1000 m, 8-day	2000–2020	LST (Terra)	Wan (2008)
TerraClimate	4000 m, monthly	1980–2020	Ta, ET _a , ET _r , VPD, SM, SR	Abatzoglou et al. (2018)
Peng_1km	1000 m, monthly	1980–2020	Ta	Peng et al. (2019)
SRTM	90 m	static	Elevation	Jarvis et al. (2008)
Water use	provincial	2002–2019	Mean irrigation water use	–
Statistical data	provincial	2000–2019	Irrigation area	–

2.3.1. Pairwise comparison based on a flexible window-searching algorithm

The pairwise comparison method is effective for evaluating the differences in ecological, hydrological, and climatic factors caused by land use and land cover changes (Li et al., 2015; Wang et al., 2021a, 2018). Like Yang et al. (2020a), we used this approach to examine the cooling effects of agricultural irrigation, as quantified by the LST difference between irrigated croplands and non-irrigated grasslands. It is commonly assumed that irrigated and non-irrigated pixels within a small extent share similar large-scale climate forcing and the nonlocal signals of background climate can be removed after the differentiation (Li et al., 2016; Xu et al., 2022). Here we adopted a flexible window-searching algorithm to delimit the irrigated pixels and nearby non-irrigated pixels at the 31×31 km scale (Yang et al., 2020a). Two other window sizes including 21×21 km and 41×41 km were also examined to test the robustness of our approach.

First, we overlaid the five NLCD data sets from 2000, 2005, 2010, 2015, and 2020 to identify pixels that were consistently cropland or grassland over the last two decades. Second, the flexible window-searching algorithm was used to identify valid irrigated pixels. Specifically, a $L_0 \times L_0$ window centered on an irrigated pixel was established and the non-irrigated pixels in this window were counted. A valid irrigated pixel was the one with at least N non-irrigated (reference) pixels and their elevation difference with the irrigated pixel was less than a

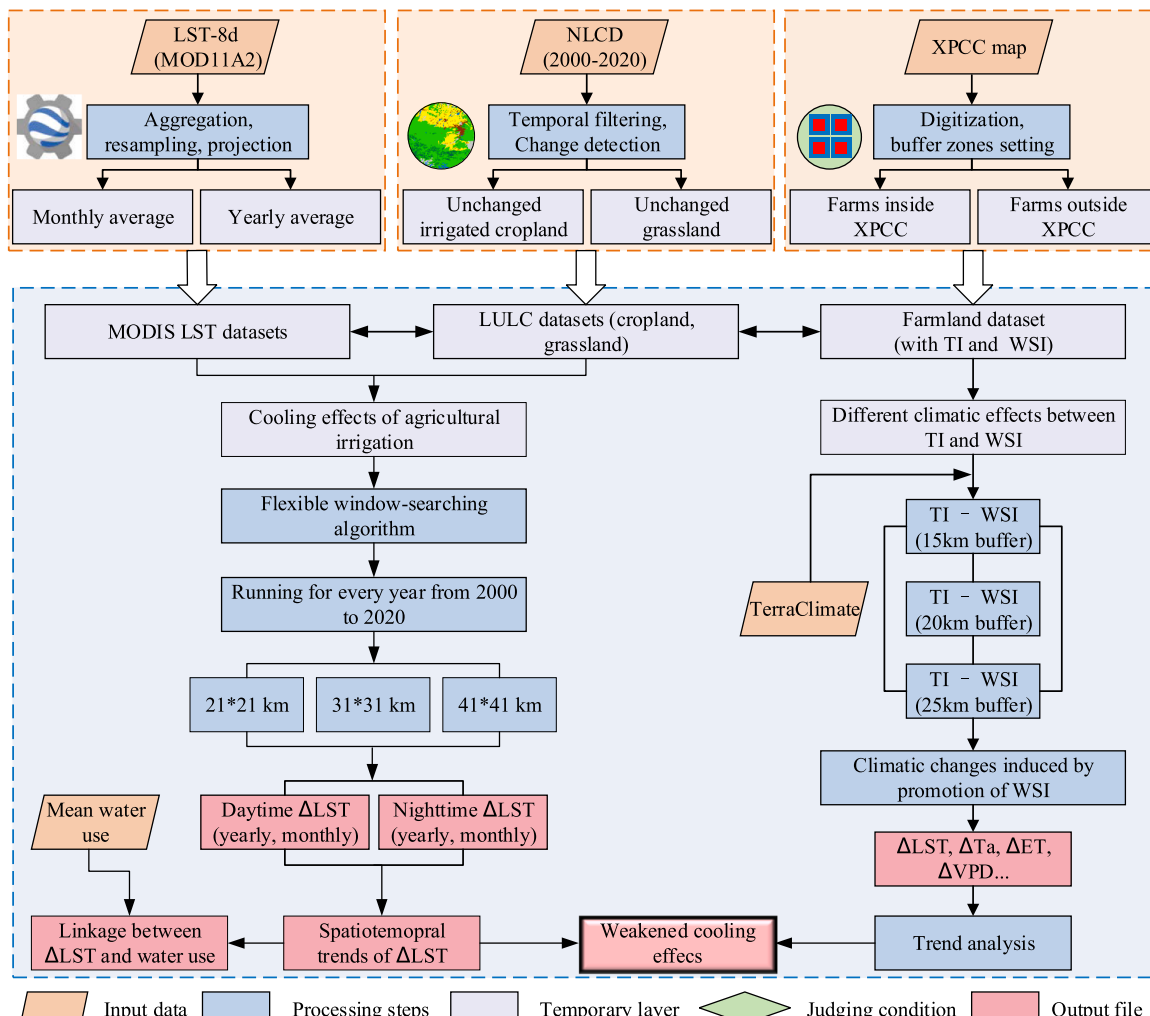


Fig. 2. Our workflow for determining changes in irrigation cooling effect and its relationship with irrigation water use. NLCD = National Land Cover Dataset of China. TI – WSI = Climatic factors of farms using traditional irrigation (TI) minus that of water-saving irrigation (WSI). The three circles inside the top row indicate the Google Earth Engine platform, a sketch map of land use/cover (yellow and green represent cropland and grassland, respectively), and a sketch map of farms (red) inside the XPCC and their buffer zones (blue), respectively. XPCC = Xinjiang Production and Construction Corps.

threshold (E). If the central irrigated pixel did not meet the criteria in the $L_0 \times L_0$ window, the window size was amplified step-by-step by 2 km, and the counting process was repeated until it met the criteria or the window edge reached a maximum length (L_{max}).

We set the above parameters as $L_0 = 31$ km, $N = 10$, $E = 50$ m, and $L_{max} = 100$ km. Other parameters were also tested to demonstrate robustness (see Section 4.4). The difference in LST between irrigated pixels and their reference non-irrigated pixels (Eq. (1)) showed the LST changes (ΔLST) induced by agricultural irrigation. A positive or negative ΔLST represents the warming or cooling effect of irrigation, respectively.

$$\Delta LST_{cooling} = LST_{irrigation} - LST_{non-irrigation} \quad (1)$$

2.3.2. Quantification of the cooling effect trends and attribution analysis

Based on the annual ΔLST time-series images from 2000 to 2020, we calculated the trend of ΔLST using linear regression at the pixel scale, quantifying the temporal pattern of ΔLST changes in the last two decades. Next, the pixel-wise ΔLST was aggregated into Xinjiang, North Xinjiang, and South Xinjiang to show the regional variations and discrepancies. In terms of temporal dimensions, we conducted the analyses at annual, seasonal, and diurnal scales.

We investigated the relationship between ΔLST changes and mean agricultural water use and climate factors (i.e., precipitation, air temperature, and solar radiation) using partial correlation analyses in both Xinjiang and its two subregions. Note that the provincial water use data was used for Xinjiang, North Xinjiang, and South Xinjiang, due to the lack of regional-specific data.

We also quantified the relative importance of water use and three climate factors to ΔLST using a dominance analysis of the multiple linear

regression model (Eq. (2)).

$$\Delta LST = b_0 + b_1 \times IWU + b_2 \times Pr + b_3 \times Ta + b_4 \times Sr + \varepsilon \quad (2)$$

where IWU , Pr , Ta , and Sr represent irrigation water use, precipitation, air temperature, and solar radiation, respectively. ε indicates other factors that may contribute to LST changes. The dominance analysis was expected to identify the individual contributions of the above four factors to ΔLST and was conducted using the Python package “dominance analysis” (https://github.com/kaladharprajapati/dominance_analysis), which is based on the decomposition of variance for multiple linear regression models. According to the dominance analyses, a higher value means higher contribution (importance) and will be identified as the dominant driver.

2.3.3. Comparison of the climatic effects between water-saving irrigation and traditional irrigation

We assumed that different irrigation methods, like traditional irrigation (channels and ditches) and WSI (drip or sprinkler), have different impacts on LST since they differ in water supply, soil moisture, and ET (Ambika and Mishra, 2022; Han et al., 2017a). Many studies reported that WSI was mainly used at XPCC farmlands before the late 1990s and was then gradually promoted outside of XPCC farmlands (Han et al., 2021; Zhang et al., 2019; Zhao et al., 1996; Zhong et al., 2009). Thus, we used these two types of farmlands to investigate the cooling effects induced by different irrigation methods (Eq. (3)). Specifically, we defined the farms equipped with WSI using the official boundaries of XPCC jurisdiction (Fig. 1a) and delimited the farms using traditional irrigation as those inside of the 20-km buffers around the XPCC. The LST difference due to irrigation methods was quantified using the LST of all

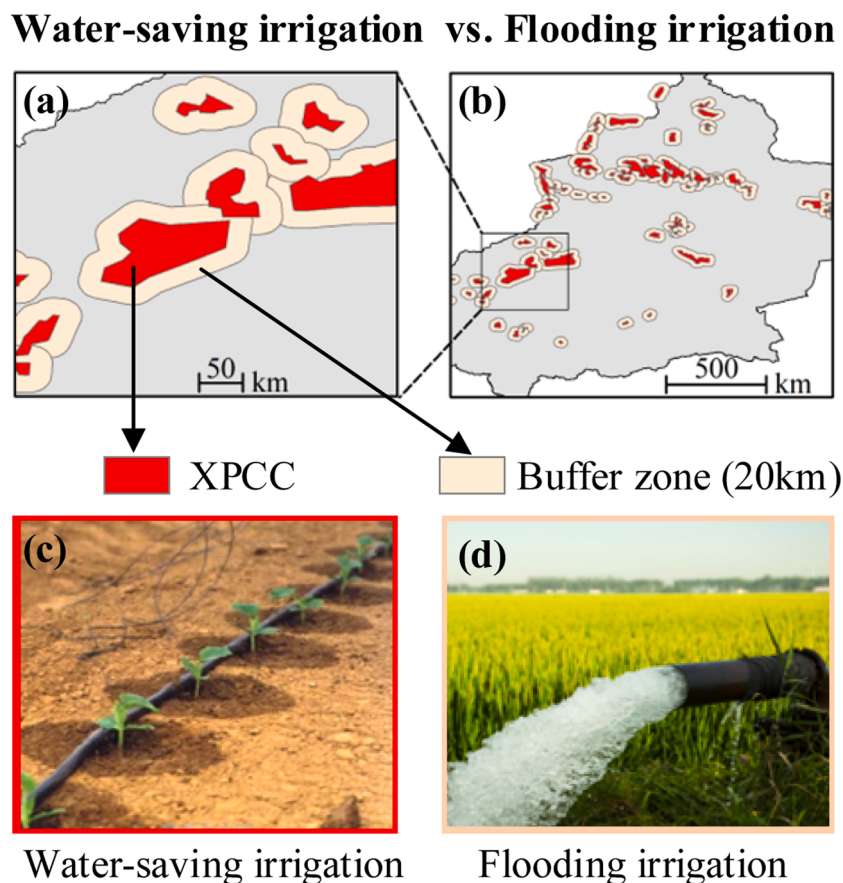


Fig. 3. Schematic of the comparison between water-saving irrigation vs. traditional irrigation (flooding) at the farm level. (a) Zoom-in view of Xinjiang Production & Construction Corps (XPCC, mean area of farms: 684 km²). (b) Full view of the XPCC. (c) and (d) indicate farmlands using water-saving and flooding irrigation methods, respectively.

cropland pixels inside the XPCC minus that inside the buffers. The schematic diagram of the comparison between WSI and traditional irrigation is shown in Fig. 3.

$$\Delta LST_{WSI-TI} = LST_{\text{water-saving irrigation}} - LST_{\text{traditional irrigation}} \quad (3)$$

Apart from MODIS daytime LST, the differences in various climatic factors from the TerraClimate dataset, including maximum air temperature (Ta), actual and reference ET (ETa and ETr), vapor pressure deficit (VPD), and soil moisture (SM), were also computed using Eq. (3). The long-term dataset from 1980 to 2020 allowed us to not only examine the climatic differences between traditional irrigation and WSI but to also observe their trends as WSI became more commonplace on conventional farms. Note that the croplands inside and outside XPCC were extracted from the NLCD dataset and each nominal year's land cover was extended to five years that included two preceding and two subsequent years (e.g., 1990 represented 1988–1992). An exception was the land cover for the 1980s, which was used for years 1980–1987.

3. Results

3.1. Spatial patterns of the changing irrigation cooling effects in Xinjiang

The difference in LST between irrigated and non-irrigated pixels was examined by pairwise comparison in 31×31 km windows and their trends were calculated to observe changes over time (Fig. 4, Fig. S3). In total, we identified 58,724 valid irrigated pixels, with 57% and 43% of them distributed in North and South Xinjiang (Fig. S4), respectively. Overall, the irrigated areas had a lower annual mean LST than non-irrigated areas both in the daytime (-2.40 K) and nighttime (-0.19 K) over the study period. Spatial discrepancies were found in ΔLST with a mean daytime cooling of -1.57 K in North Xinjiang and -3.46 K in South Xinjiang. The cooling effects of irrigated croplands changed extensively since 2000 with 31% of them having a significantly positive trend ($p < 0.1$) in the daytime (Fig. 4b), which indicated that the

daytime cooling effect weakened with time. The attenuated daytime cooling effect was more prominent in South Xinjiang than in North Xinjiang, where the proportion of significantly positive trends was 31% and 16%, respectively (Fig. 4c), probably due to the larger area of WSI in South Xinjiang and will be discussed in the following sections. In contrast, 32% of the irrigated croplands showed a significantly negative trend ($p < 0.1$) in the nighttime (Fig. S3b), indicating the aggravated nighttime cooling effect. The intensified nighttime cooling was more evident in North Xinjiang than in South Xinjiang (proportions of significantly negative trends: 19% vs. 13%, Fig. S3c).

3.2. Changing cooling effects of irrigation at annual, seasonal, and diurnal scales

We aggregated the pixel-wise ΔLST into three regions (i.e., Xinjiang, North Xinjiang, and South Xinjiang) and calculated their temporal trends at annual, seasonal, and diurnal scales, respectively. As Fig. 5 illustrated, the mean annual daytime ΔLST in Xinjiang significantly increased with a trend of 0.208 K/decade ($p < 0.05$), indicating a weakened daytime cooling effect. Regionally, South Xinjiang had a steeper trend in annual daytime ΔLST of 0.482 K/decade ($p < 0.05$), and no significant trend was found in North Xinjiang (slope = 0.004 , $p > 0.1$). In terms of nighttime ΔLST changes, all three regions had a clear intensified cooling trend, among which North Xinjiang had the steepest trend (-0.130 K/decade, $p < 0.05$), followed by Xinjiang (-0.117 K/decade, $p < 0.05$) and South Xinjiang (-0.100 K/decade, $p < 0.1$). The annual ΔLST trends evidently correlated to mean irrigation water use with asymmetric characteristics. Daytime ΔLST magnitude was magnified and nighttime ΔLST magnitude was reduced with increasing irrigation water use (Fig. 5c, d), meaning that less water use due to WSI could alleviate the daytime cooling effect and intensify the nighttime cooling effect. The correlation relationships were significant ($p < 0.1$) at all regional scales except North Xinjiang, which may be due to the confounding effect of background climate like precipitation and will be

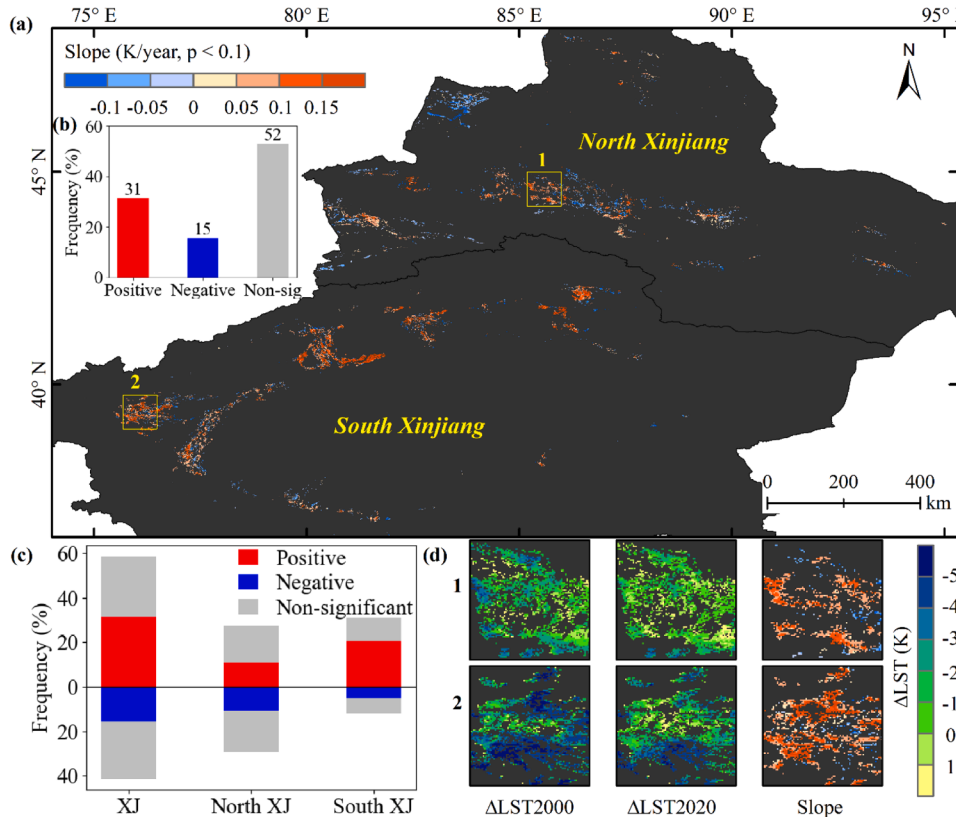


Fig. 4. Pixelwise daytime cooling trends of irrigated croplands in Xinjiang from 2000 to 2020 (a). (b) Frequency of pixels with significantly positive and negative and non-significantly changed trends across Xinjiang. (c) Same as (b) but displayed by dividing the pixels with non-significant trends into positive and negative groups for Xinjiang, North Xinjiang, and South Xinjiang. (d) Zoom-in plots of cooling patterns in 2000 (ΔLST_{2000}) and 2020 (ΔLST_{2020}), and the trends of cooling effects. All slope pixels shown in (a) and (d) meet $p < 0.1$ based on Student's t -test. XJ = Xinjiang.

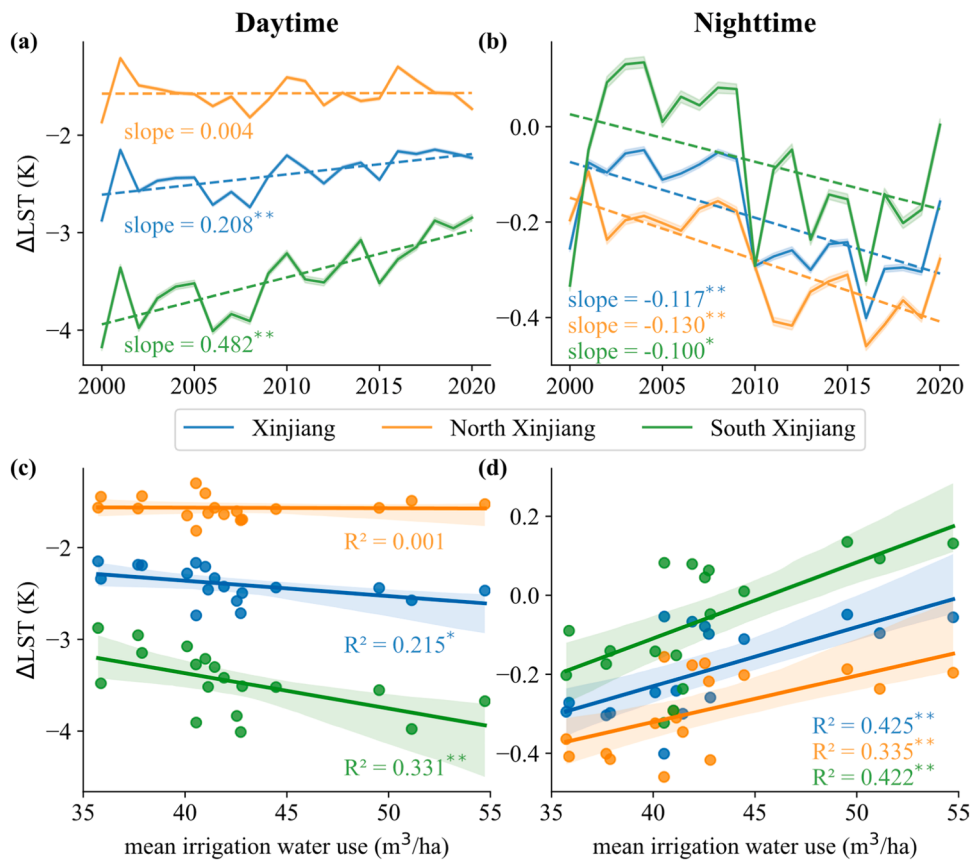


Fig. 5. The annual cooling trends (K/decade) of croplands in Xinjiang, North Xinjiang, and South Xinjiang from 2000 to 2020 for the daytime (a) and nighttime (b). Mean irrigation water use versus land surface temperature change (ΔLST) in the daytime (c) and nighttime (d). * represents $p < 0.1$ and ** represents $p < 0.05$ based on Student's t -test. The shadows represent 95% confidence intervals.

further investigated in the next section.

We also calculated the daytime and nighttime mean ΔLST for each month for seasonal analysis from 2000 to 2020 (Fig. 6). The irrigation cooling effect was most evident in the growing season (from May to September) with a mean daytime cooling of -4.19 K (Table S1) and nighttime cooling of -0.47 K (Table S2) for Xinjiang, and was especially strong in July and August. South Xinjiang had a higher daytime cooling magnitude than North Xinjiang in nearly all months. For the nighttime, South Xinjiang had contrasting seasonal effects with warming in spring and winter, and cooling in summer and autumn, while North Xinjiang always had a slight nighttime cooling effect in all seasons. In the nighttime, the ground surface releases energy stored in the daytime and heats the atmosphere (Chen and Jeong, 2018), but this heating effect will be mediated or surpassed by the enhanced latent flux in the intensively irrigated growing season (in South Xinjiang) or relatively humid environment (in North Xinjiang) (Fig. 6b). In terms of cooling trends, daytime ΔLST in most months in Xinjiang decreased, which was more evident in spring and autumn. Regionally, the weakened daytime cooling trend was more marked in South Xinjiang, and the increased nighttime cooling pattern was more evident in North Xinjiang, which may be due to their different irrigation extents and intensities.

3.3. Attribution analyses of the changing irrigation cooling effects

In general, the LST is tightly coupled with soil moisture, ET, and albedo (Liu et al., 2019; Qiu et al., 2022; Shen et al., 2019; Zeng et al., 2021), which are affected by irrigation and background climates like precipitation, air temperature, and solar radiation (Pitman et al., 2011). In Xinjiang, the average water use for agricultural irrigation has decreased from $11505\text{ m}^3/\text{ha}$ in 2002 to $8481\text{ m}^3/\text{ha}$ in 2019 at a rate of

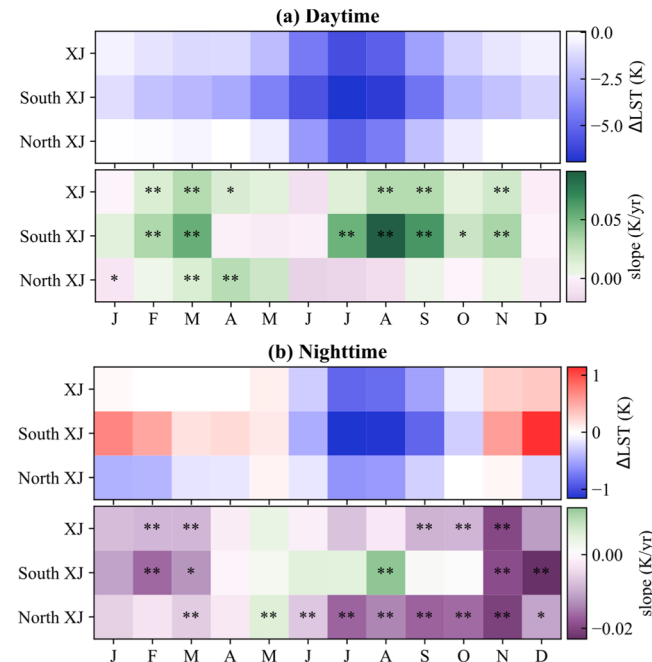


Fig. 6. Monthly mean ΔLST and ΔLST trends of croplands in Xinjiang, South Xinjiang, and North Xinjiang from 2000 to 2020 during the daytime (a) and nighttime (b). * represents $p < 0.1$ and ** represents $p < 0.05$ based on Student's t -test. XJ = Xinjiang.

$-177.3 \text{ m}^3/\text{ha}$ per year (Fig. 1d). Here we quantified the relationship between the temporal changes of cooling effects and mean irrigation water use (IWU) and three climate factors using partial correlation analysis.

As illustrated in Fig. 7, both daytime and nighttime ΔLST were significantly correlated with the mean IWU ($p < 0.05$) in Xinjiang, North Xinjiang, and South Xinjiang after controlling the climate factors. Declining IWU dominated ΔLST changes with a contribution of more than 30% at all regional and temporal scales except in North Xinjiang in the daytime (7.7%, Fig. 7c, Table S4). Contrasting diurnal correlations between ΔLST with IWU were found and were characterized by a negative correlation in the daytime and a positive correlation in the nighttime. Specifically, the daytime ΔLST in South Xinjiang was more negatively correlated with IWU than in North Xinjiang (partial correlation coefficient: -0.688 vs. -0.544 , $p < 0.05$, Table S3). Note that precipitation played a more important role than IWU in North Xinjiang in the daytime (partial correlation coefficient: 0.603 vs. -0.544 and relative importance: 38.9% vs. 7.3% , Fig. 7a, c) since precipitation is relatively higher and the WSI area is less compared to South Xinjiang (Fig. 1c). In contrast, nighttime ΔLST was positively correlated with IWU at all regional scales, which indicated that the nighttime cooling effect intensified as IWU decreased (Fig. 5d). This aggravated trend may be related to the decreased soil moisture and increased albedo in the daytime (because of brighter soil color). Since the land surface assimilates solar radiation in the daytime and releases energy at night (Li et al., 2015), less energy absorbed in the daytime (due to increased albedo) can be dissipated in the nighttime, thus intensifying the nighttime cooling effect (Peng et al., 2014). Regionally, the nighttime ΔLST in South Xinjiang was slightly more correlated with IWU than in North Xinjiang (partial correlation coefficient: 0.790 vs. 0.740 , $p < 0.05$).

3.4. Different climatic effects of traditional and water-saving irrigation at the field scale

Using XPCC farms and non-XPCC farms (Fig. 1a, Fig. 3), we

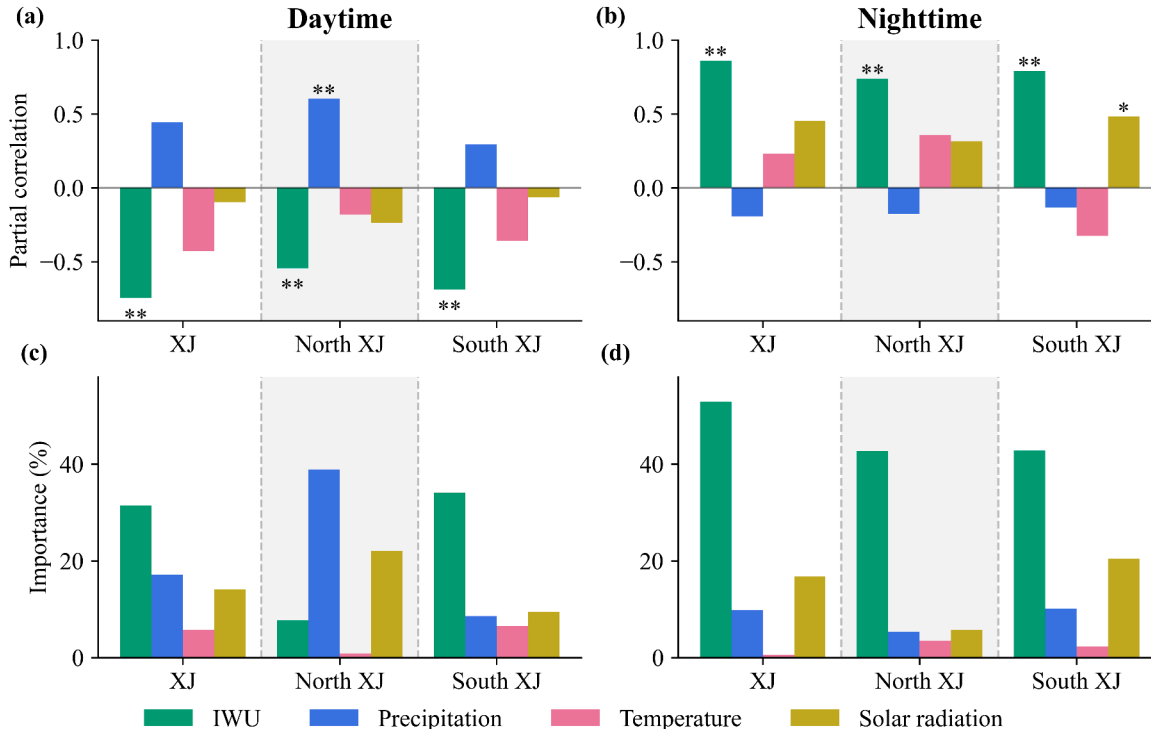


Fig. 7. Partial correlation and dominance analyses of four factors (i.e., irrigation water use (IWU), precipitation, temperature, and incoming solar radiation) with ΔLST changes. (a, b) Partial correlation analyses for daytime and nighttime. (c, d) Variable importance of four factors for daytime and nighttime. * represents $p < 0.1$ and ** represents $p < 0.05$ based on Student's t -test. XJ = Xinjiang.

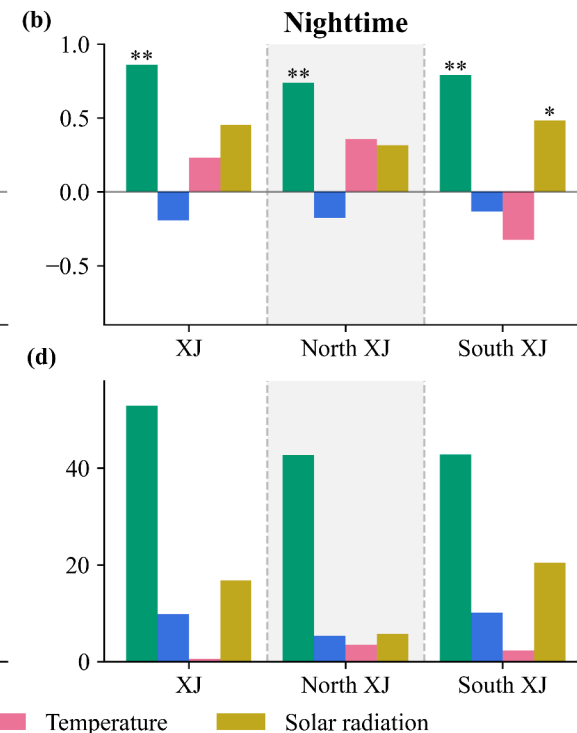
compared daytime LST (from MODIS) and several other climatic factors (from TerraClimate) of traditional irrigation and WSI lands, respectively. As shown in Fig. 8, both daytime LST and Ta of farms using WSI methods were significantly higher ($p < 0.001$) than farms using traditional irrigation methods (Fig. 8a, b). The annual daytime ΔLST had a markedly larger magnitude than ΔTa (mean value of 0.430 K vs. 0.031 K for 2000–2020). In addition, the farms using WSI had larger VPD and ETr, and lower ETa and SM than conventional farms. The gaps between the climatic effects of WSI and traditional irrigation were dynamic over the last four decades and we found a turning point in 1998. The WSI had a higher Ta (mean: 0.055 K) with a slightly upward trend than traditional irrigation before 1998 but ΔTa had a downward trend ($-0.026 \text{ K}/\text{decade}$, $p < 0.001$) after 1998 and gradually converged to 0 in 2020.

Similar patterns can be found in the trend of ΔVPD (Fig. 8c), ΔETr (Fig. 8d), ΔETA (Fig. 8e), and ΔSM (Fig. 8f). All the temporal trends were significant ($p < 0.1$) except for ΔSM after 1998, possibly due to complicated climate conditions like extreme precipitation and drought. The climatic differences (i.e., LST, Ta, VPD, Eta, ETr) between the two kinds of farms can be attributed to the different irrigation methods they adopted (Han et al., 2017a). The different trends before and after 1998 may be due to the different development stages and area proportions of WSI inside and outside of XPCC, which we discussed in Section 4.3.

4. Discussion

4.1. Declining cooling effects of irrigated croplands in Xinjiang

Previous studies have demonstrated that the irrigation cooling effect is dominated by increased ET as a consequence of additional water supply (Liu et al., 2019, 2022; Yang et al., 2020b). Compared to the non-irrigated areas, more energy is transformed into latent heat flux due to the additional water supply from the irrigation, thus reducing the sensible heat flux for heating the air. Such a cooling effect is particularly pronounced in arid regions, especially in Xinjiang, where the potential ET is generally high (Han et al., 2017b). Based on our results, most of the



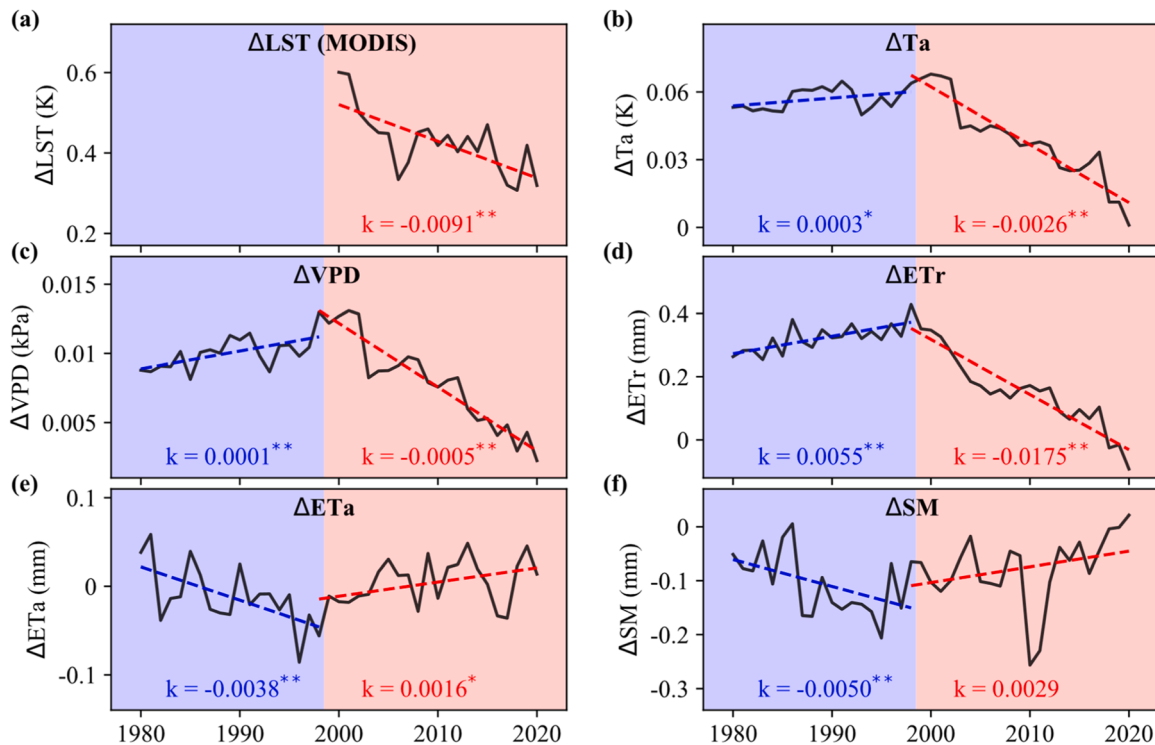


Fig. 8. Differences in multiple climate factors between the farms inside and outside (20-km buffer) of Xinjiang Production and Construction Corps (XPCC) jurisdiction from 1980 to 2020, including daytime ΔLST (a), air temperature (Ta) (b), ΔVPD (c), ΔETr (reference ET) (d), ΔETa (actual ET) (e), and ΔSM (soil moisture) (f). All data is from the TerraClimate except LST (MODIS). The blue and red spaces represent before and after the year 1998. Simple linear regressions are implemented for the time series before (blue dotted line) and after 1998 (red dotted line), respectively. The k and p denote the slope and p -value of the trend, respectively. Daytime ΔLST before 2000 is absent due to the unavailability of MODIS LST data. * represents $p < 0.1$ and ** represents $p < 0.05$ based on Student's t -test.

irrigated croplands in Xinjiang had a weakened daytime cooling effect from 2000 to 2020 (Fig. S4) and the mean annual decrease was 0.64 K with a slope of 0.21 K/decade. Also, the relationship between annual ΔLST and mean water use for irrigation was significantly correlated both in the daytime and nighttime.

Limited by the dry climate and scarce water resources in Xinjiang, WSI techniques were introduced and developed due to policies and subsidies from the central and local governments (Fig. 9). The gross area of croplands under WSI expanded from 1266 ha in 2000 to 2916 ha in 2019, and the corresponding mean water use for irrigation fell by over

26% (Fig. 1d). As an advanced irrigation technique, WSI technology like drip irrigation under plastic films or mulches only supplies water to roots through lines with small holes, which reduces water use to a large extent. Fu et al. (2022b) reported that substantial improvements in irrigation efficiency have reduced irrigation water demand per unit area by over 60% and saved irrigation water of 18.5 billion m³ from 1990 to 2015 in Tarim Basin, Xinjiang. As a result, the soil water content and ET activity of WSI are obviously less than that of traditional flood irrigation (Han et al., 2017a). Moreover, a slight increase in potential ET and a decrease in actual ET trends were found in the cropland area over the

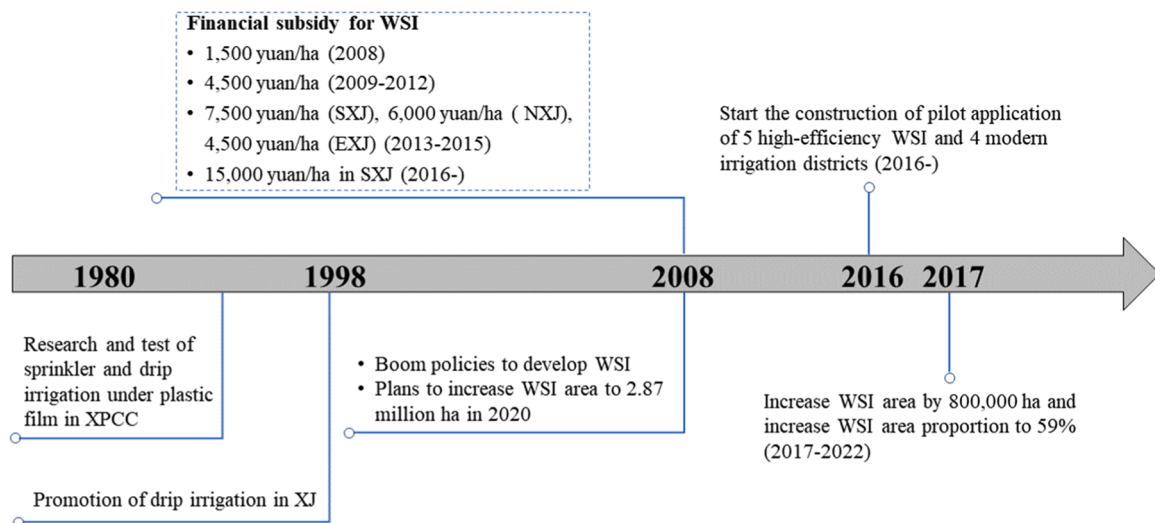


Fig. 9. Stimulus policies relevant to the development of water-saving irrigation (WSI). SXJ, NXJ, and EXJ indicate South, North, and East Xinjiang, respectively. XPCC = Xinjiang Production and Construction Corps.

period 1990–2015 (Fu et al., 2022b).

4.2. Spatial and temporal discrepancies of the weakened cooling effects

The overall weakened cooling effects in Xinjiang from 2000 to 2020 had both spatial (i.e., North Xinjiang and South Xinjiang) and temporal (seasonal and diurnal) discrepancies. The attenuated daytime cooling trend was intensive in South Xinjiang but negligible in North Xinjiang, probably due to different advancements in WSI and differences in background environmental conditions between the two regions. South Xinjiang has a drier climate with less precipitation and water resources than North Xinjiang (Fig. S2), which challenged the sustainability of agricultural irrigation (Yao et al., 2022a). Thus, the demand for developing WSI is stronger in South Xinjiang than in North Xinjiang. According to the official report, the area of high-efficiency WSI increased by 583,500 ha in South Xinjiang from 2016 to 2020, almost three times the new WSI area in North Xinjiang (Fig. 9). On the contrary, North Xinjiang, especially the north slope of Tianshan Mountain, has relatively abundant water resources, which negates the demand for WSI. As a result, the mean IWU per hectare in North Xinjiang may be larger than in South Xinjiang. In addition, the more humid climate in North Xinjiang could also lead to smaller irrigation cooling effects than in South Xinjiang (Yang et al., 2020a), and the corresponding weakened trend was not evident.

We also found apparent diurnal and seasonal discrepancies in the cooling trends in both North Xinjiang and South Xinjiang. The diurnal cooling trends were asymmetric in the last two decades, characterized by mitigated daytime cooling and intensified nighttime cooling. Less water supply usually leads to reduced soil moisture and ET and higher soil albedo than traditional irrigation (Fu et al., 2022b; Zhang et al., 2020b). Reduced soil moisture and ET could dampen the daytime cooling effect. In general, the land surface absorbs and stores energy from the atmosphere during the daytime and releases heat in the nighttime (Lee et al., 2011). At night, ET is negligible, and LST must be closely related to the energy stored during the daytime (Peng et al., 2014). Higher albedo means less solar radiation (energy) will be absorbed; therefore, less heat can be dissipated at nighttime, enhancing the nighttime cooling trends. In addition, the decrease in surface heat capacity because of less daytime heat storage (lower soil moisture) may lead to a reduction of air humidity near the surface and a decrease in boundary layer cloud formation. As a result, less downward longwave radiation is received from the atmosphere and more longwave radiation is emitted from the ground surface (Zhou et al., 2007). This longwave radiative imbalance has a stronger effect at night than during the daytime (Dai et al., 1999), which also leads to intensified nighttime cooling trends.

As for the seasonal patterns, the significantly weakened daytime cooling was concentrated in late summer and early spring, which corresponded to the two major stages of irrigation (Han and Yang, 2013). Crop growth in late summer needs more water, and thus this period has the most intensive cooling effects during the year, and the weakened cooling magnitude would be more marked than in other seasons. In the early spring, irrigation is usually used to leach salt and conserve soil moisture (Han et al., 2017a), and is thus accompanied by slightly mitigated cooling trends.

4.3. Different climatic effects between farms using traditional irrigation and WSI

Since WSI techniques were first tested and promoted on XPCC farms in the late 1970s, the proportion of WSI peaked when non-XPCC farms began to adopt and encourage WSI in the late 1990s and early 2000s. As a result, farms with WSI had a lower ET_a and SM than that with traditional irrigation and the gap magnitude showed an increasing trend from 1980 to 1998 (Fig. 8e, f), despite some disturbances due to data uncertainty. Correspondingly, the lower soil moisture and ET of XPCC

farms led to a higher temperature than non-XPCC farms, and the difference had a slightly upward trend before 1998 due to the gap in irrigation methods (Fig. S5).

Thanks to the stimulus and subsidy policies from the central and local governments, WSI systems were promoted to farms outside of XPCC jurisdiction in the late 1990s and developed rapidly. Thus, the gap in irrigation techniques between these farms decreased, and the differences in temperature and other climatic factors had a downward trend after 1998. A most recent study reported that water-saving technologies increased irrigation efficiency in the source of the Tarim Basin by 17% from 0.3 in 1990 to 0.35 in 2000, accompanied by faster growth in later years (49% increase from 0.35 in 2000 to 0.52 in 2015) (Fu et al., 2022b). The different growth velocities before and after 2000 partly corroborate the varied development phases of WSI in state farms and conventional farms. Furthermore, our results were consistent with Han et al.'s studies (Han et al., 2021, 2017a), which found different temporal trends of potential evapotranspiration before and after 1998 in Xinjiang based on in situ observations. In addition to using the 20-km buffers to identify non-XPCC farms, we also tested 15-km and 25-km buffers (Fig. S6, Fig. S7.) and found that our results were consistent. Moreover, we replaced Ta from the TerraClimate dataset with that from Peng 1 km dataset and found a similar declining trend of Δ Ta after 1998 between farms inside and outside the XPCC (Fig. S8), demonstrating the robustness of our results. Our findings provide new evidence of the effect of WSI practices on climate under the background of an increasingly warming and wetting climate in northwest China (Yao et al., 2022a).

4.4. Sensitivity tests, uncertainties, and implications

In this study, we delineated the spatiotemporal patterns of irrigation cooling effects and their relationship with water use changes at different scales in Xinjiang in the last two decades. Compared to a recent study that delineated the WSI-induced warming effect in northwest India using WRF simulations (Ambika and Mishra, 2022), our study reflected the actual climate changes due to WSI promotion, immune to the uncertainties from model parameterization or coarse-resolution irrigation dataset. Furthermore, relative to a similar study in northwest China based on in situ observations (Fu et al., 2022a), the adoption of satellite observations here, which have a spatially explicit nature and frequent revisit, allowed us to uncover the representative pattern of WSI-induced indirect warming effect based on analyses at multi-spatiotemporal scales. The adoption of all stable irrigated croplands allowed us to examine the change in mean cooling effects with more and more croplands adopting WSI techniques, eliminating the impact of newly expanded croplands. The flexible window-searching algorithm effectively extracts the LST difference between irrigation and non-irrigation areas. Although the window size was flexible from 31 km to 100 km to enhance valid grids, more than 80% of the windows had a 31 km size (Fig. S9). In addition to the parameters that we adopted ($L_0 = 31$ km, $N = 10$, $E = 50$ m, and $L_{max} = 100$ km), we also tested other values like $L_0 = 21$ km, 41 km, $N = 15, 20, 25$, and $E = 60$ m, 80 m, 100 m (Fig. S10, Fig. S11). The sensitivity tests demonstrated that our method was robust and insensitive to different parameter values.

Nevertheless, some aspects can be improved. First is the bias from the data quality of the MODIS dataset (e.g., LST), which is susceptible to cloud contamination (Li et al., 2015; Shen et al., 2020) and may introduce some uncertainties into our results. Further, the land use and land cover data may also have some misclassifications (Sevcikova and Nichols, 2021). However, we adopted the 20-year averaged map which was expected to improve the reliability. Second, we attributed the mitigated cooling effects of irrigated croplands to the implementation of WSI, since the partial correlation analysis showed a good causal relationship between mean water use and Δ LST. However, some other factors (i.e., precipitation and solar radiation) may also play a role in affecting Δ LST changes at regional scales, such as precipitation in North Xinjiang and solar radiation in South Xinjiang (Fig. 7). Yang et al.

(2020a) reported that enhanced precipitation would dampen the irrigation cooling effect because the additional water supplied by irrigation has a weaker impact on the land surface in the humid climate zone than in the arid climate zone. This phenomenon was evident in North Xinjiang due to its relatively higher precipitation than in South Xinjiang. In addition, the attenuated cooling effect of WSI revealed by this study was a low boundary because it may be partly counteracted by vegetation greening, which is closely related to vegetation ET activity (Cui et al., 2022; Lian et al., 2022; Piao et al., 2020; Shen et al., 2022a, 2022b). For instance, Forzieri et al. (2017) reported that vegetation greening with increased LAI contributed to evaporation-driven cooling in arid regions and the interplay between LAI and surface biophysics is amplified up to five times under extreme warm-dry and cold-wet years. Yu et al. (2022) found an evident daytime cooling effect induced by crop greening during the growing season in Northeast China. In our future work, regional climate models assisted by in situ observations will be utilized to quantify more drivers and feedback of the WSI effect.

Third, due to the lack of finer-scale (e.g., county or prefecture-scale) IWU data, we used provincial-level data to investigate the relationship between cooling dynamics and water use changes for North and South Xinjiang, which may introduce some unmanageable uncertainties. Furthermore, the provincial water use data corresponds to all croplands including both stable and new irrigated croplands, which may impair its explanatory power for the weakened cooling effect. But even so, we could find a significant correlation between the changes in the cooling effect and water use, and we believe the explanatory power would be higher with the availability of finer-scale data.

Fourth, when exploring the climatic differences between state farms (inside of XPCC) and conventional farms (outside of XPCC), we did not consider the different cropping structures and other management strategies between these farms due to the data unavailability, since different crop types and management methods may have different climatic effects (Liu et al., 2022; Luyssaert et al., 2014). Moreover, some uncertainties may be introduced when using the TerraClimate dataset to retrieve the WSI effects because some XPCC scales are too small to reflect the difference in temperature between farms inside and outside the XPCC. In the future, a comprehensive comparison of the climatic discrepancies between traditional irrigation and WSI should be implemented with more explicit and solid information about the cropland types, mean water uses, climate and soil conditions. In addition, future studies can investigate more biophysical effects of WSI including relative humidity, wet bulb temperature, and moist heat stress using climate models (i.e., WRF).

5. Conclusions

High-efficiency WSI techniques have expanded rapidly in Xinjiang in recent decades but WSI expansion-induced impacts on local and regional climates remain rarely investigated. We investigated the impact of increased WSI on LST from 2000 to 2020 using the pairwise comparison method at the pixel and farm scales. We found a clear weakened cooling effect of irrigation over the croplands in Xinjiang in the last two decades. For the first time, we observed the cooling trend had a contrasting diurnal cycle with mitigated daytime cooling and intensified nighttime cooling. The declined daytime cooling had a markedly larger magnitude than the intensified nighttime cooling and thus dominated the overall weakened daily cooling trend. Regionally, the weakened cooling was significant in South Xinjiang but not so in North Xinjiang. Seasonally, the weakened cooling effect was more significant in late summer and early spring than in the other seasons.

Decreased mean water use for irrigation could have reduced the daytime Δ LST but intensified the nighttime Δ LST. Through our comparison between XPCC farmlands with WSI and non-XPCC farmlands with traditional irrigation, we further confirmed that the WSI has a weaker cooling effect than traditional irrigation, but the difference in the cooling effect between the two farmlands narrowed with the rapid

expansion of WSI. Our findings provide new insights into the effects of WSI on climate in northwest China in the last two decades and inform future modeling and climate adaptation efforts.

CRediT authorship contribution statement

Chao Zhang: Conceptualization, Methodology, Formal analysis, Writing – original draft. **Jinwei Dong:** Supervision, Conceptualization, Writing – review & editing. **Guoyong Leng:** Writing – review & editing. **Russell Doughty:** Writing – review & editing. **Kun Zhang:** Writing – review & editing. **Songjun Han:** Conceptualization, Validation. **Geli Zhang:** Writing – review & editing. **Xuezhen Zhang:** Writing – review & editing. **Quansheng Ge:** Supervision, Conceptualization.

Declaration of Competing Interest

The authors declare that they have no known competing financial interests or personal relationships that could have appeared to influence the work reported in this paper.

Data availability

Data will be made available on request.

Acknowledgment

This study was supported by the Strategic Priority Research Program (Grant No. XDA28060100, XDA23100400), the CAS Youth Interdisciplinary Team Project (Grant No. JCTD-2021-04) of the Chinese Academy of Sciences, and the National Natural Science Foundation of China (Grant No. 41871349, 42271375).

Supplementary materials

Supplementary material associated with this article can be found, in the online version, at doi:10.1016/j.agrformet.2023.109397.

References

- Abatzoglou, J.T., Dobrowski, S.Z., Parks, S.A., Hegewisch, K.C., 2018. TerraClimate, a high-resolution global dataset of monthly climate and climatic water balance from 1958 to 2015. *Sci. Data* 5, 170191–170202. <https://doi.org/10.1038/sdata.2017.191>.
- Ambika, A.K., Mishra, V., 2019. Observational evidence of irrigation influence on vegetation health and land surface temperature in India. *Geophys. Res. Lett.* 46, 13441–13451. <https://doi.org/10.1029/2019GL084367>.
- Ambika, A.K., Mishra, V., 2021. Modulation of compound extremes of low soil moisture and high vapor pressure deficit by irrigation in India. *J. Geophys. Res.: Atmos.* 126, e2021JD034529 <https://doi.org/10.1029/2021jd034529>.
- Ambika, A.K., Mishra, V., 2022. Improved water savings and reduction in moist heat stress caused by efficient irrigation. *Earth's Fut.* 10, e2021EF002642 <https://doi.org/10.1029/2021EF002642>.
- Bin Abdullah, K., 2006. Use of water and land for food security and environmental sustainability. *Irrig. Drain.* 55, 219–222. <https://doi.org/10.1002/ird.254>.
- Chen, L., Dirmeyer, P.A., 2019. Global observed and modelled impacts of irrigation on surface temperature. *Int. J. Climatol.* 39, 2587–2600. <https://doi.org/10.1002/joc.5973>.
- Chen, X., Jeong, S.-J., 2018. Irrigation enhances local warming with greater nocturnal warming effects than daytime cooling effects. *Environ. Res. Lett.* 13, 024005 <https://doi.org/10.1088/1748-9326/aa9dea>.
- Cui, J., Lian, X., Huntingford, C., Gimeno, L., Wang, T., Ding, J., He, M., Xu, H., Chen, A., Gentile, P., Piao, S., 2022. Global water availability boosted by vegetation-driven changes in atmospheric moisture transport. *Nat. Geosci.* <https://doi.org/10.1038/s41561-022-01061-7>.
- Dai, A., Trenberth, K.E., Karl, T.R., 1999. Effects of clouds, soil moisture, precipitation, and water vapor on diurnal temperature range. *J. Clim.* 12, 2451–2473. [https://doi.org/10.1175/1520-0442\(1999\)012<2451:Eocsmr>2.0.Co;2](https://doi.org/10.1175/1520-0442(1999)012<2451:Eocsmr>2.0.Co;2).
- Deng, X.-P., Shan, L., Zhang, H., Turner, N.C., 2006. Improving agricultural water use efficiency in arid and semiarid areas of China. *Agric. Water Manag.* 80, 23–40. <https://doi.org/10.1016/j.agwat.2005.07.021>.
- Forzieri, G., Alkama, R., Miralles, D.G., Cescatti, A., 2017. Satellites reveal contrasting responses of regional climate to the widespread greening of Earth. *Science* 356, 1180–1184. <https://doi.org/10.1126/science.aal1727>.

- Fu, J., Kang, S., Zhang, L., Li, X., Gentine, P., Niu, J., 2022a. Amplified warming induced by large-scale application of water-saving techniques. *Environ. Res. Lett.* 17, 034018 <https://doi.org/10.1088/1748-9326/ac4b52>.
- Fu, J., Wang, W., Zaitchik, B., Nie, W., Fei, E.X., Miller, S.M., Harman, C.J., 2022b. Critical role of irrigation efficiency for cropland expansion in Western China arid agroecosystems. *Earth's Future* 10, e2022EF002955. <https://doi.org/10.1029/2022EF002955>.
- Gorelick, N., Hancher, M., Dixon, M., Ilyushchenko, S., Thau, D., Moore, R., 2017. Google Earth Engine: planetary-scale geospatial analysis for everyone. *Remote Sens. Environ.* 202, 18–27. <https://doi.org/10.1016/j.rse.2017.06.031>.
- Han, C., Zhang, B., Han, S., 2021. Quantitative effects of changes in agricultural irrigation on potential evaporation. *Hydrol. Processes* 35, e14057. <https://doi.org/10.1002/hyp.14057>.
- Han, S., Yang, Z., 2013. Cooling effect of agricultural irrigation over Xinjiang, Northwest China from 1959 to 2006. *Environ. Res. Lett.* 8, 024039 <https://doi.org/10.1088/1748-9326/8/2/024039>.
- Han, S., Xu, D., Yang, Z., 2017a. Irrigation-induced changes in evapotranspiration demand of Awati Irrigation District, Northwest China: weakening the effects of water saving? *Sustainability* 9 1531. <https://doi.org/10.3390/su9091531>.
- Han, S., Tang, Q., Xu, D., Wang, S., Yang, Z., 2017b. Observed near-surface atmospheric moisture content changes affected by irrigation development in Xinjiang, Northwest China. *Theor. Appl. Climatol.* 130, 511–521. <https://doi.org/10.1007/s00704-016-1899-2>.
- Jägermeyer, J., Gerten, D., Heinke, J., Schaphoff, S., Kummu, M., Lucht, W., 2015. Water savings potentials of irrigation systems: global simulation of processes and linkages. *Hydrol. Earth Syst. Sci.* 19, 3073–3091. <https://doi.org/10.5194/hess-19-3073-2015>.
- Jarvis, A., H.I. Reuter, A. Nelson, E. Guevara, 2008. Hole-filled SRTM for the globe: version 4: data grid, available from the CGIAR-CSI SRTM 90m database: <http://srtm.cgiar.org>. (Accessed 27 December 2021).
- Kamran, M., Yan, Z., Ahmad, I., Jia, Q., Ghani, M.U., Chen, X., Chang, S., Li, T., Siddique, K.H.M., Fahad, S., Hou, F., 2023. Assessment of greenhouse gases emissions, global warming potential and net ecosystem economic benefits from wheat field with reduced irrigation and nitrogen management in an arid region of China. *Agric. Ecosyst. Environ.* 341, 108197 <https://doi.org/10.1016/j.agee.2022.108197>.
- Kitzberger, T., Tiribelli, F., Barbera, I., Haridas Gowda, J., Manuel Morales, J., Zalazar, L., Paritis, J., 2022. Projections of fire probability and ecosystem vulnerability under 21st century climate across a trans-Andean productivity gradient in Patagonia. *Sci. Total Environ.* 839 <https://doi.org/10.1016/j.scitotenv.2022.156303>.
- Kueppers, L.M., Snyder, M.A., Sloan, L.C., 2007. Irrigation cooling effect: regional climate forcing by land-use change. *Geophys. Res. Lett.* 34 <https://doi.org/10.1029/2006gl028679>.
- Lee, X., Goulden, M.L., Hollinger, D.Y., Barr, A., Black, T.A., Bohrer, G., Bracho, R., Drake, B., Goldstein, A., Gu, L., Katul, G., Kolb, T., Law, B.E., Margolis, H., Meyers, T., Monson, R., Munger, W., Oren, R., Paw U, K.T., Richardson, A.D., Schmid, H.P., Staebler, R., Wofsy, S., Zhao, L., 2011. Observed increase in local cooling effect of deforestation at higher latitudes. *Nature* 479, 384–387. <https://doi.org/10.1038/nature10588>.
- Li, L., Zeng, Z., Zhang, G., Duan, K., Liu, B., Cai, X., 2022. Exploring the individualized effect of climatic drivers on MODIS net primary productivity through an explainable machine learning framework. *Remote Sens.* 14, 4401.
- Li, Y., Zhao, M., Motesharrei, S., Mu, Q., Kalnay, E., Li, S., 2015. Local cooling and warming effects of forests based on satellite observations. *Nat. Commun.* 6, 6603. <https://doi.org/10.1038/ncomms7603>.
- Li, Y., Zhao, M., Mildrexler, D.J., Motesharrei, S., Mu, Q., Kalnay, E., Zhao, F., Li, S., Wang, K., 2016. Potential and actual impacts of deforestation and afforestation on land surface temperature. *J. Geophys. Res.: Atmos.* 121 (14), 372. <https://doi.org/10.1002/2016JD024969>. -314386.
- Lian, X., Jeong, S., Park, C.-E., Xu, H., Li, L.Z.X., Wang, T., Gentine, P., Peñuelas, J., Piao, S., 2022. Biophysical impacts of northern vegetation changes on seasonal warming patterns. *Nat. Commun.* 13, 3925. <https://doi.org/10.1038/s41467-022-31671-z>.
- Liu, G., Wang, W., Shao, Q., Wei, J., Zheng, J., Liu, B., Chen, Z., 2021. Simulating the climatic effects of irrigation over China by using the WRF-noah model system with mosaic approach. *J. Geophys. Res.: Atmos.* 126, e2020JD034428 <https://doi.org/10.1029/2020JD034428>.
- Liu, J., Liu, M., Tian, H., Zhuang, D., Zhang, Z., Zhang, W., Tang, X., Deng, X., 2005. Spatial and temporal patterns of China's cropland during 1990–2000: an analysis based on Landsat TM data. *Remote Sens. Environ.* 98, 442–456. <https://doi.org/10.1016/j.rse.2005.08.012>.
- Liu, J., Zhang, Z., Xu, X., Kuang, W., Zhou, W., Zhang, S., Li, R., Yan, C., Yu, D., Wu, S., Jiang, N., 2010. Spatial patterns and driving forces of land use change in China during the early 21st century. *J. Geog. Sci.* 20, 483–494. <https://doi.org/10.1007/s11442-010-0483-4>.
- Liu, J., Kuang, W., Zhang, Z., Xu, X., Qin, Y., Ning, J., Zhou, W., Zhang, S., Li, R., Yan, C., Wu, S., Shi, X., Jiang, N., Yu, D., Pan, X., Chi, W., 2014. Spatiotemporal characteristics, patterns, and causes of land-use changes in China since the late 1980s. *J. Geog. Sci.* 24, 195–210. <https://doi.org/10.1007/s11442-014-1082-6>.
- Liu, T., Yu, L., Zhang, S., 2019. Impacts of wetland reclamation and paddy field expansion on observed local temperature trends in the Sanjiang Plain of China. *J. Geophys. Res.: Earth Surf.* 124, 414–426. <https://doi.org/10.1029/2018JF004846>.
- Liu, W., Dong, J., Du, G., Zhang, G., Hao, Z., You, N., Zhao, G., Flynn, K.C., Yang, T., Zhou, Y., 2022. Biophysical effects of paddy rice expansion on land surface temperature in Northeastern Asia. *Agric. For. Meteorol.* 315, 108820 <https://doi.org/10.1016/j.agrformet.2022.108820>.
- Lobell, D., Bala, G., Mirin, A., Phillips, T., Maxwell, R., Rotman, D., 2009. Regional differences in the influence of irrigation on climate. *J. Clim.* 22, 2248–2255. <https://doi.org/10.1175/2008jcli2703.1>.
- Lobell, D.B., Bonfils, C., 2008. The effect of irrigation on regional temperatures: a spatial and temporal analysis of trends in California, 1934–2002. *J. Clim.* 21, 2063–2071. <https://doi.org/10.1175/2007jcli1755.1>.
- Lu, Y., Harding, K., Kueppers, L., 2017. Irrigation effects on land–atmosphere coupling strength in the United States. *J. Clim.* 30, 3671–3685. <https://doi.org/10.1175/jcli-d-15-0706.1>.
- Luyssaert, S., Jammet, M., Stoy, P.C., Estel, S., Pongratz, J., Ceschia, E., Churkina, G., Don, A., Erb, K., Ferlioq, M., Gielen, B., Grünwald, T., Houghton, R.A., Klumpp, K., Knöhl, A., Kolb, T., Kuemmerle, T., Laurila, T., Lohila, A., Loustau, D., McGrath, M. J., Meyfroidt, P., Moors, E.J., Naudts, K., Novick, K., Otto, J., Pilegaard, K., Pio, C.A., Rambal, S., Rebmann, C., Ryder, J., Suyker, A.E., Varlagin, A., Wattenbach, M., Dolman, A.J., 2014. Land management and land-cover change have impacts of similar magnitude on surface temperature. *Nat. Clim. Change* 4, 389–393. <https://doi.org/10.1038/nclimate2196>.
- Mahmood, R., Hubbard, K.G., Carlson, C., 2004. Modification of growing-season surface temperature records in the northern great plains due to land-use transformation: verification of modelling results and implication for global climate change. *Int. J. Climatol.* 24, 311–327. <https://doi.org/10.1002/joc.992>.
- Mahmood, R., Foster, S.A., Keeling, T., Hubbard, K.G., Carlson, C., Leeper, R., 2006. Impacts of irrigation on 20th century temperature in the northern Great Plains. *Global Planet. Change* 54, 1–18. <https://doi.org/10.1016/j.gloplacha.2005.10.004>.
- Ministry of Water Resources, P.R.C., 2021. China Water Statistical Yearbook 2021. China WaterPower Press, Beijing.
- Molden, D., Oweis, T., Steduto, P., Bindraban, P., Hanjra, M.A., Kijne, J., 2010. Improving agricultural water productivity: between optimism and caution. *Agric. Water Manage.* 97, 528–535. <https://doi.org/10.1016/j.agwat.2009.03.023>.
- Nocco, M.A., Smail, R.A., Kucharik, C.J., 2019. Observation of irrigation-induced climate change in the Midwest United States. *Glob Chang Biol* 25, 3472–3484. <https://doi.org/10.1111/gcb.14725>.
- Peng, S.-S., Piao, S., Zeng, Z., Ciais, P., Zhou, L., Li, L.Z.X., Myneni, R.B., Yin, Y., Zeng, H., 2014. Afforestation in China cools local land surface temperature. *Proc. Natl. Acad. Sci. U.S.A.* 111, 2915–2919. <https://doi.org/10.1073/pnas.1315126111>.
- Peng, S., Ding, Y., Liu, W., Li, Z., 2019. 1 km monthly temperature and precipitation dataset for China from 1901 to 2017. *Earth Syst. Sci. Data* 11, 1931–1946. <https://doi.org/10.5194/essd-11-1931-2019>.
- Piao, S., Wang, X., Park, T., Chen, C., Lian, X., He, Y., Bjerke, J.W., Chen, A., Ciais, P., Tømmervik, H., Nemani, R.R., Myneni, R.B., 2020. Characteristics, drivers and feedbacks of global greening. *Nat. Rev. Earth Environ.* 1, 14–27. <https://doi.org/10.1038/s43017-019-0001-x>.
- Pitman, A.J., Avila, F.B., Abramowitz, G., Wang, Y.P., Phipps, S.J., de Noblet-Ducoudré, N., 2011. Importance of background climate in determining impact of land-cover change on regional climate. *Nat. Clim. Change* 1, 472–475. <https://doi.org/10.1038/nclimate1294>.
- Puma, M.J., Cook, B.I., 2010. Effects of irrigation on global climate during the 20th century. *J. Geophys. Res.* 115, D16120. <https://doi.org/10.1029/2010jd014122>.
- Puy, A., Borgonovo, E., Lo Piano, S., Levin, S.A., Saltelli, A., 2021. Irrigated areas drive irrigation water withdrawals. *Nat. Commun.* 12, 4525. <https://doi.org/10.1038/s41467-021-24508-8>.
- Qi, X., Feng, K., Sun, L., Zhao, D., Huang, X., Zhang, D., Liu, Z., Baiocchi, G., 2022. Rising agricultural water scarcity in China is driven by expansion of irrigated cropland in water scarce regions. *One Earth* 5, 1139–1152. [https://doi.org/10.1016/j.onear.2022.09.008](https://doi.org/10.1016/j.oneear.2022.09.008).
- Qiu, J., Crow, W.T., Wang, S., Dong, J., Li, Y., Garcia, M., Shangguan, W., 2022. Microware-based soil moisture improves estimates of vegetation response to drought in China. *Sci. Total Environ.* 849, 157535 <https://doi.org/10.1016/j.scitotenv.2022.157535>.
- Sacks, W.J., Cook, B.I., Buennning, N., Lewis, S., Helkowski, J.H., 2009. Effects of global irrigation on the near-surface climate. *Clim. Dyn.* 33, 159–175. <https://doi.org/10.1007/s00382-008-0445-z>.
- Sevcikova, H., Nichols, B., 2021. Land use uncertainty in transportation forecast. *J. Transp. Land Use* 14, 805–820. <https://doi.org/10.5198/jtlu.2021.1853>.
- Shen, W., Li, M., Huang, C., He, T., Tao, X., Wei, A., 2019. Local land surface temperature change induced by afforestation based on satellite observations in Guangdong plantation forests in China. *Agric. For. Meteorol.* 276–277. <https://doi.org/10.1016/j.agrformet.2019.107641>.
- Shen, X., Liu, B., Jiang, M., Lu, X., 2020. Marshland loss warms local land surface temperature in China. *Geophys. Res. Lett.* 47, e2020GL087648 <https://doi.org/10.1029/2020GL087648>.
- Shen, X., Liu, B., Henderson, M., Wang, L., Jiang, M., Lu, X., 2022a. Vegetation greening, extended growing seasons, and temperature feedbacks in warming temperate grasslands of China. *J. Clim.* 1–51. <https://doi.org/10.1175/jcli-D-21-0325.1>.
- Shen, X., Liu, B., Jiang, M., Wang, Y., Wang, L., Zhang, J., Lu, X., 2021. Spatiotemporal change of marsh vegetation and its response to climate change in China from 2000 to 2019. *J. Geophys. Res.: Biogeosci.* 126, e2020JG006154 <https://doi.org/10.1029/2020JG006154>.
- Shen, X., Liu, Y., Wu, L., Ma, R., Wang, Y., Zhang, J., Wang, L., Liu, B., Lu, X., Jiang, M., 2022b. Grassland greening impacts on global land surface temperature. *Sci. Total Environ.*, 155851 <https://doi.org/10.1016/j.scitotenv.2022.155851>.
- Stahl, M.O., McColl, K.A., 2022. The seasonal cycle of surface soil moisture. *J. Clim.* 35, 4997–5012. <https://doi.org/10.1175/jcli-D-21-0780.1>.

- Thierry, W., Visser, A.J., Fischer, E.M., Hauser, M., Hirsch, A.L., Lawrence, D.M., Lejeune, Q., Davin, E.L., Seneviratne, S.I., 2020. Warming of hot extremes alleviated by expanding irrigation. *Nat. Commun.* 11 <https://doi.org/10.1038/s41467-019-14075-4>.
- Wan, Z., 2008. New refinements and validation of the MODIS land-surface temperature/emissivity products. *Remote Sens. Environ.* 112, 59–74. <https://doi.org/10.1016/j.rse.2006.06.026>.
- Wang, C., Li, S., Wu, M., Jansson, P.-E., Zhang, W., He, H., Xing, X., Yang, D., Huang, S., Kang, D., He, Y., 2022. Modelling water and energy fluxes with an explicit representation of irrigation under mulch in a maize field. *Agric. For. Meteorol.* 326, 109145 <https://doi.org/10.1016/j.agrformet.2022.109145>.
- Wang, J., Xiao, X., Zhang, Y., Qin, Y., Doughty, R.B., Wu, X., Bajgain, R., Du, L., 2018. Enhanced gross primary production and evapotranspiration in juniper-encroached grasslands. *Global Change Biol.* 24, 5655–5667. <https://doi.org/10.1111/gcb.14441>.
- Wang, J., Xiao, X., Basara, J., Wu, X., Bajgain, R., Qin, Y., Doughty, R.B., Iii, B.M., 2021a. Impacts of juniper woody plant encroachment into grasslands on local climate. *Agric. For. Meteorol.* 307, 108508 <https://doi.org/10.1016/j.agrformet.2021.108508>.
- Wang, W., Liu, G., Wei, J., Chen, Z., Ding, Y., Zheng, J., 2021b. The climatic effects of irrigation over the middle and lower reaches of the Yangtze River, China. *Agric. For. Meteorol.* 308–309. <https://doi.org/10.1016/j.agrformet.2021.108550>, 108550.
- Wu, B., Tian, F., Zhang, M., Piao, S., Zeng, H., Zhu, W., Liu, J., Elnashar, A., Lu, Y., 2022a. Quantifying global agricultural water appropriation with data derived from earth observations. *J. Clean. Prod.* 358, 131891 <https://doi.org/10.1016/j.jclepro.2022.131891>.
- Wu, C., Peng, J., Ciais, P., Peñuelas, J., Wang, H., Beguería, S., Andrew Black, T., Jassal, R.S., Zhang, X., Yuan, W., Liang, E., Wang, X., Hua, H., Liu, R., Ju, W., Fu, Y., H., Ge, Q., 2022b. Increased drought effects on the phenology of autumn leaf senescence. *Nat. Clim. Change.* <https://doi.org/10.1038/s41558-022-01464-9>.
- Xin, F., Xiao, X., Dong, J., Zhang, G., Zhang, Y., Wu, X., Li, X., Zou, Z., Ma, J., Du, G., Doughty, R.B., Zhao, B., Li, B., 2020. Large increases of paddy rice area, gross primary production, and grain production in Northeast China during 2000–2017. *Sci. Total Environ.* 711, 135183–135192. <https://doi.org/10.1016/j.scitotenv.2019.135183>.
- Xu, R., Li, Y., Teuling, A.J., Zhao, L., Spracklen, D.V., Garcia-Carreras, L., Meier, R., Chen, L., Zheng, Y., Lin, H., Fu, B., 2022. Contrasting impacts of forests on cloud cover based on satellite observations. *Nat. Commun.* 13 (670) <https://doi.org/10.1038/s41467-022-28161-7>.
- Xu, X., Zhang, M., Li, J., Liu, Z., Zhao, Z., Zhang, Y., Zhou, S., Wang, Z., 2018. Improving water use efficiency and grain yield of winter wheat by optimizing irrigations in the North China Plain. *Field Crops Res.* 221, 219–227. <https://doi.org/10.1016/j.fieldcrops.2018.02.011>.
- Yang, D., Li, S., Wu, M., Yang, H., Zhang, W., Chen, J., Wang, C., Huang, S., Zhang, R., Zhang, Y., 2023. Drip irrigation improves spring wheat water productivity by reducing leaf area while increasing yield. *Eur. J. Agron.* 143, 126710 <https://doi.org/10.1016/j.eja.2022.126710>.
- Yang, Q., Huang, X., Tang, Q., 2020a. Irrigation cooling effect on land surface temperature across China based on satellite observations. *Sci. Total Environ.* 705, 135984 <https://doi.org/10.1016/j.scitotenv.2019.135984>.
- Yang, Q.Q., Huang, X., Tang, Q.H., 2020b. Global assessment of the impact of irrigation on land surface temperature. *Sci. Bull.* 65, 1440–1443. <https://doi.org/10.1016/j.scib.2020.04.005>.
- Yang, Y. (2019). Xinjiang water resources bulletin (2006–2012). In C. National Tibetan Plateau Data (Ed.): National Tibetan Plateau Data Center.
- Yao, J., Chen, Y., Guan, X., Zhao, Y., Chen, J., Mao, W., 2022a. Recent climate and hydrological changes in a mountain–basin system in Xinjiang, China. *Earth Sci. Rev.* 226, 103957. <https://doi.org/10.1016/j.earscirev.2022.103957>.
- Yao, Y., Vanderkelen, I., Lombardozzi, D., Swenson, S., Lawrence, D., Jägermeyr, J., Grant, L., Thiery, W., 2022b. Implementation and evaluation of irrigation techniques in the community land model. *J. Adv. Model. Earth Syst.* 14, e2022MS003074 <https://doi.org/10.1029/2022MS003074>.
- Yu, L., Liu, Y., Yang, J., Liu, T., Bu, K., Li, G., Jiao, Y., Zhang, S., 2022. Asymmetric daytime and nighttime surface temperature feedback induced by crop greening across Northeast China. *Agric. For. Meteorol.* 325, 109136 <https://doi.org/10.1016/j.agrformet.2022.109136>.
- Zeng, Z., Wang, D., Yang, L., Wu, J., Ziegler, A.D., Liu, M., Ciais, P., Searchinger, T.D., Yang, Z.-L., Chen, D., Chen, A., Li, L.Z.X., Piao, S., Taylor, D., Cai, X., Pan, M., Peng, L., Lin, P., Gower, D., Feng, Y., Zheng, C., Guan, K., Lian, X., Wang, T., Wang, L., Jeong, S.-J., Wei, Z., Sheffield, J., Caylor, K., Wood, E.F., 2021. Deforestation-induced warming over tropical mountain regions regulated by elevation. *Nat. Geosci.* 14, 23–29. <https://doi.org/10.1038/s41561-020-00666-0>.
- Zhang, C., Dong, J., Ge, Q., 2022a. Quantifying the accuracies of six 30-m cropland datasets over China: a comparison and evaluation analysis. *Comput. Electron. Agric.* 197, 106946 <https://doi.org/10.1016/j.compag.2022.106946>.
- Zhang, C., Dong, J., Ge, Q., 2022b. IrriMap.CN: annual irrigation maps across China in 2000–2019 based on satellite observations, environmental variables, and machine learning. *Remote Sens. Environ.* 280, 113184 <https://doi.org/10.1016/j.rse.2022.113184>.
- Zhang, C., Dong, J., Ge, Q., 2022c. Mapping 20 years of irrigated croplands in China using MODIS and statistics and existing irrigation products. *Sci. Data* 9 (407). <https://doi.org/10.1038/s41597-022-01522-z>.
- Zhang, C., Dong, J., Zuo, L., Ge, Q., 2022d. Tracking spatiotemporal dynamics of irrigated croplands in China from 2000 to 2019 through the synergy of remote sensing, statistics, and historical irrigation datasets. *Agric. Water Manage.* 263, 107458–107470. <https://doi.org/10.1016/j.agwat.2022.107458>.
- Zhang, C., Dong, J., Xie, Y., Zhang, X., Ge, Q., 2022e. Mapping irrigated croplands in China using a synergistic training sample generating method, machine learning classifier, and Google Earth Engine. *Int. J. Appl. Earth Obs. Geoinf.* 112, 102888 <https://doi.org/10.1016/j.jag.2022.102888>.
- Zhang, G., Xiao, X., Dong, J., Xin, F., Zhang, Y., Qin, Y., Doughty, R.B., Moore 3rd, B., 2020a. Fingerprint of rice paddies in spatial-temporal dynamics of atmospheric methane concentration in monsoon Asia. *Nat. Commun.* 11, 554–564. <https://doi.org/10.1038/s41467-019-14155-5>.
- Zhang, G., Liu, C., Xiao, C., Xie, R., Ming, B., Hou, P., Liu, G., Xu, W., Shen, D., Wang, K., Li, S., 2017a. Optimizing water use efficiency and economic return of super high yield spring maize under drip irrigation and plastic mulching in arid areas of China. *Field Crops Res.* 211, 137–146. <https://doi.org/10.1016/j.fcr.2017.05.026>.
- Zhang, G., Xiao, X., Biradar, C.M., Dong, J., Qin, Y., Menarguez, M.A., Zhou, Y., Zhang, Y., Jin, C., Wang, J., Doughty, R.B., Ding, M., Moore 3rd, B., 2017b. Spatiotemporal patterns of paddy rice croplands in China and India from 2000 to 2015. *Sci. Total Environ.* 579, 82–92. <https://doi.org/10.1016/j.scitotenv.2016.10.223>.
- Zhang, K., Li, X., Zheng, D., Zhang, L., Zhu, G., 2022f. Estimation of Global Irrigation Water Use by the Integration of Multiple Satellite Observations. *Water Resour. Res.* 58, e2021WR030031 <https://doi.org/10.1029/2021WR030031>.
- Zhang, X., Xiong, Z., Tang, Q., 2017c. Modeled effects of irrigation on surface climate in the Heihe River Basin, Northwest China. *J. Geophys. Res.: Atmos.* 122, 7881–7895. <https://doi.org/10.1002/2017jd026732>.
- Zhang, X., Ding, N., Han, S., Tang, Q., 2020b. Irrigation-induced potential evapotranspiration decrease in the Heihe River Basin, Northwest China, as simulated by the WRF model. *J. Geophys. Res.: Atmos.* 125 <https://doi.org/10.1029/2019jd031058>.
- Zhang, X., Yang, L., Xue, X., Kamran, M., Ahmad, I., Dong, Z., Liu, T., Jia, Z., Zhang, P., Han, Q., 2019. Plastic film mulching stimulates soil wet-dry alternation and stomatal behavior to improve maize yield and resource use efficiency in a semi-arid region. *Field Crops Res.* 233, 101–113. <https://doi.org/10.1016/j.fcr.2019.01.002>.
- Zhang, Z., Lin, A., Zhao, L., Zhao, B., 2022g. Attribution of local land surface temperature variations response to irrigation over the North China Plain. *Sci. Total Environ.* 826, 154104 <https://doi.org/10.1016/j.scitotenv.2022.154104>.
- Zhang, C., Ge, Q., Dong, J., Zhang, X., Li, Y., Han, S., 2023. Characterizing spatial, diurnal, and seasonal patterns of agricultural irrigation expansion-induced cooling in Northwest China from 2000 to 2020. *Agric. For. Meteorol.* 330, 109304 <https://doi.org/10.1016/j.agrformet.2022.109304>.
- Zhang, Z., Hu, H., Tian, F., Yao, X., Sivapalan, M., 2014. Groundwater dynamics under water-saving irrigation and implications for sustainable water management in an oasis: tarim River basin of western China. *Hydrol. Earth Syst. Sci.* 18, 3951–3967. <https://doi.org/10.5194/hess-18-3951-2014>.
- Zhao, R., Li, B., Zhang, Z., 1996. The present situation and prospect of water saving irrigation in Xinjiang (in Chinese). *J. Xinjiang Agric. Univ.* 19 (3), 52–55.
- Zhong, R., Dong, X., Ma, Y., 2009. Sustainable water saving: new concept of modern agricultural water saving, starting from development of Xinjiang's agricultural irrigation over the last 50 years. *Irrig. Drain.* 58, 383–392. <https://doi.org/10.1002/ird.414>.
- Zhong, R., Tian, F., Yang, P., Yi, Q., 2016. Planting and irrigation methods for cotton in Southern Xinjiang, China. *Irrig. Drain.* 65, 461–468. <https://doi.org/10.1002/ird.2015>.
- Zhou, D., Li, D., Sun, G., Zhang, L., Liu, Y., Hao, L., 2016. Contrasting effects of urbanization and agriculture on surface temperature in eastern China. *J. Geophys. Res.* 121, 9597–9606. <https://doi.org/10.1029/2016JD025359>.
- Zhou, D., Xiao, J., Frolking, S., Liu, S., Zhang, L., Cui, Y., Zhou, G., 2021a. Croplands intensify regional and global warming according to satellite observations. *Remote Sens. Environ.* 264, 112585 <https://doi.org/10.1016/j.rse.2021.112585>.
- Zhou, F., Bo, Y., Ciais, P., Dumas, P., Tang, Q., Wang, X., Liu, J., Zheng, C., Polcher, J., Yin, Z., Guimbretieau, M., Peng, S., Ottle, C., Zhao, X., Zhao, J., Tan, Q., Chen, L., Shen, H., Yang, H., Piao, S., Wang, H., Wada, Y., 2020. Deceleration of China's human water use and its key drivers. *Proc. Natl. Acad. Sci.* 117, 7702–7711. <https://doi.org/10.1073/pnas.1909902117>.
- Zhou, L., Dickinson, R.E., Tian, Y., Vose, R.S., Dai, Y., 2007. Impact of vegetation removal and soil aridation on diurnal temperature range in a semiarid region: application to the Sahel. *Proc. Natl. Acad. Sci. U.S.A.* 104, 17937–17942. <https://doi.org/10.1073/pnas.0700290104>.
- Zhou, X., Zhang, Y., Sheng, Z., Manevski, K., Andersen, M.N., Han, S., Li, H., Yang, Y., 2021b. Did water-saving irrigation protect water resources over the past 40 years? A global analysis based on water accounting framework. *Agric. Water Manage.* 249, 106793 <https://doi.org/10.1016/j.agwat.2021.106793>.